# Modeling Autogenous Pressurization and Draining of a Cryogenic Storage Tank in Normal Gravity

Olga Kartuzova[1] and Mohammad Kassemi[2]
*National Center for Space Exploration Research (NCSER), Case Western Reserve University and NASA Glenn Research Center, Cleveland, OH 44135, USA*
Daniel Hauser[3]
*NASA Glenn Research Center, Cleveland, OH 44135, USA*

**A two-phase CFD model for autogenous pressurization and draining of a cryogenic storage tank is presented using both the Sharp Interface and Volume-Of-Fluid (VOF) approaches for capturing the front and the associated interfacial heat, mass and momentum transfer between the liquid and vapor regions. Both models are validated against data provided by the Cryogenic Propellant Storage and Transfer (CPST) Engineering Development Unit (EDU) experiment[1]. The results of the autogenous pressurization are presented first, focusing on the phase change and turbulence effects on the tank pressure and temperature predictions. Both the Sharp Interface (SI-CFD) and VOF (VOF-CFD) multiphase models predict tank pressure during pressurization within 3% of the measured values. The sensitivity of key physical and numerical parameters of the problem are tested using the Sharp Interface model. Effects of the accommodation coefficient (AC), and the computational grid structure are studied. The second part of this paper is devoted to validating the SI-VOF model, with an enhanced capability of moving the liquid-vapor interface, against the draining segment of the EDU experiment. The VOF-CFD model was also used to simulate tank draining and its results were compared with the results of the Sharp Interface model with the moving interface. Both models predict tank pressure during draining within 3.5% of the measured values. Pressure decrease rate is underpredicted by both models during the first 100 seconds of draining but matches the experimental rate for the rest of the simulation.**

## Nomenclature

| | | |
|---|---|---|
| *AC* | = | accommodation coefficient |
| *E* | = | energy, J |
| F | = | force, N |
| **g** | = | gravitational acceleration, m/s$^2$ |
| *h* | = | enthalpy, J/kg |
| *k* | = | thermal conductivity, W/m·K |
| MT | = | mass transfer |
| mtr | = | mass transfer rate, kg/s |
| ***n*** | = | normal vector |
| *p, P* | = | pressure, Pa |
| *r* | = | surface curvature, m |
| *S* | = | source term |
| SI, SHI | = | Sharp Interface |

[1] Research Assistant Professor, Department of Mechanical & Aerospace Engineering, and AIAA Member.
[2] Research Professor, Department of Mechanical & Aerospace Engineering, AIAA Associate Fellow.
[3] Fluids Engineer, Fluid and Cryogenic Systems Branch.

$t$ = time, seconds
T = temperature, K
**v** = velocity, m/s
VOF = Volume of Fluid

*Greek*
$\alpha$ = cell value of volume fraction
$\mu$ = dynamic viscosity, Pa·s
$\rho$ = density, kg/m$^3$
σ = surface tension, N/m

*Subscripts*
*eff* = effective
*i* = interface
*q* = phase

## I. Introduction

Efficient cryogenic fluid management of high energy propellants is in the critical path of nearly all the NASA future human exploration mission scenarios[2]. Autogenous pressurization of the propellant in tanks uses self-generated gas to pressurize liquid propellant to keep it at the required pressure necessary to feed a rocket's engine. This method, in comparison to the traditional method of pressurization using other gasses, such as helium, offers risk reduction benefits, as well as an increased payload capacity. Conducting large scale cryogenic fluid management experiments is very expensive. Computational models designed for simulating cryogenic fluid flow, heat transfer and phase change can aid in designing future cryogenic propellant systems, however such models must be extensively validated.

In the Summer of 2014 tank pressurization tests were conducted on the Engineering Development Unit (EDU) located at Test Stand 300 at NASA Marshall Space Flight Center (MSFC). EDU is a ground based Cryogenic Fluid Management (CFM) test article supported by NASA Glenn Research Center (GRC) and MSFC. In these tests, a 150 ft$^3$ propellant tank was filled with liquid nitrogen (LN2). Autogenous pressurization tests were performed along with tests using helium gas as pressurant. Both exposed (in the ullage) and submerged diffuser configurations were tested[1]. Autogenous tank pressurization and draining experiments in the EDU tank were selected to perform model validation in the current study.

In the past computational models of various sophistication have been developed for predicting pressurization performance of cryogenic fuel tanks. An overview of such studies is given by von Rüden[3]. In 2021 Ciccotosto and Hauser[4] used the STAR-CCM+ commercial CFD code to model autogenous pressurization experiment with the EDU tank. They used two different two-phase flow modeling approaches – Sharp Interface (SI) and VOF. While the SI approach resulted in good agreement with the measured tank pressures during pressurization (within 1.4% with the experimental data), tank pressure was substantially under-predicted in the VOF approach with phase change. Adnani and Jennings[5] utilized the FLUENT CFD code to model tank pressurization. Lumped liquid, active vapor approach was used in this study. They validated their model by comparing predicted tank pressures with the results of the Delta III X-Stage tests and demonstrated good agreement.

The objective of the present study is to assess the ability of the current CFD model to accurately predict autogenous pressurization and draining of a cryogenic storage tank in normal gravity by comparing CFD results with the data provided by the EDU experiments. The results of two different approaches to modeling two-phase flow using the SI-CFD and VOF-CFD models are compared in both the pressurization and draining cases. Effects of interfacial mass transfer (accommodation coefficient) and turbulence are studied in the autogenous pressurization case with the Sharp Interface model.

## II.Test setup

The testing was conducted at MSFC's Test Stand 300 in the Summer of 2014. In the experiment the tank is approximately 1.7 m in diameter and has an estimated volume of 4.287 m$^3$. The aluminum tank wall is 6 mm thick. The tank is wrapped in Multi-Layer Insulation (MLI). In the test chosen for validation gaseous N2 was supplied through a diffuser at the top of the tank. During the draining portion of the test the diffuser was turned off and liquid N2 was drained through a Screen Channel Liquid Acquisition Device (shown in grey in Figure 1). The tank was

equipped with temperature sensors on a vertical rake, horizontal rake and on the tank wall. Tank fill level was documented using the capacitance probe data. Radio Frequency Mass Gauging (RFMG) was also performed.

## III.Mathematical Model

### A. Governing Equations

Fluid flow and heat transfer in the tank are described in terms of the continuity, Navier-Stokes and energy equations for both phases:

$$\frac{\partial \rho}{\partial t} + \nabla(\rho \mathbf{v}) = 0, \tag{1}$$

$$\frac{\partial}{\partial t}(\rho \mathbf{v}) + \nabla(\rho \mathbf{v}\mathbf{v}) = -\nabla p + \nabla\left[\mu_{eff}(\nabla \mathbf{v} + \nabla \mathrm{v}^T)\right] + \rho \mathbf{g} + \mathbf{F}_{vol}, \tag{2}$$

$$\frac{\partial}{\partial t}(\rho E) + \nabla\big(\mathbf{v}(\rho E + p)\big) = \nabla\big(k_{eff} \nabla T\big) + S_h. \tag{3}$$

In the present study, the liquid phase is treated as incompressible with variable temperature-dependent properties, except for density. The liquid density is allowed to vary linearly with temperature in the body force term of the momentum equation according to the Boussinesq approximation. The vapor is modeled as a compressible ideal gas. In the VOF-CFD model, the movement of the interface is captured diffusely using the VOF method, as promogulated by Hirt and Nichols[6]. Interfacial energy, momentum and mass balances are applied using source terms in the diffuse interfacial region.

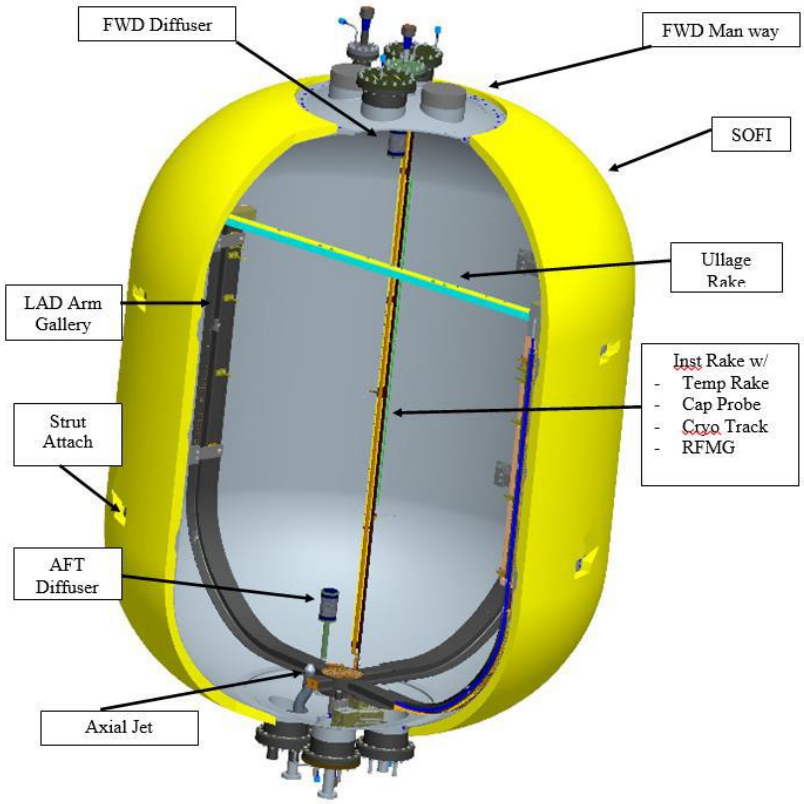


**Figure 1: EDU Tank Schematic (from Page, 2019[1])**

### B. VOF Model

In the VOF method, a volume fraction is defined in each cell such that the volume fractions of all the phases sum to unity. In the cell, the change in the interface can be tracked by solving a continuity equation for the volume fraction of the $q^{th}$ phase:

$$\frac{1}{\rho_q}\left[\frac{\partial}{\partial t}(\alpha_q \rho_q) + \nabla \cdot (\alpha_q \rho_q \mathbf{v}_q) = S_{\alpha_q}\right], \tag{4}$$

where the volume fraction for the primary phase is determined from:

$$\sum_{q=1}^{n} \alpha_q = 1. \tag{5}$$

In the VOF method, the field variables and properties are defined in terms of the volume fraction, which for a general system can be written as:

$$\rho = \sum_{q=1}^{n} \alpha_q \rho_q, \qquad \mu_{eff} = \sum_{q=1}^{n} \alpha_q \mu_{eff_q}, \qquad k_{eff} = \sum_{q=1}^{n} \alpha_q k_{eff_q}. \tag{6}$$

In this fashion, the continuity, momentum and energy equations, as described by Eq. (1) – (3), can be solved throughout the domain for the temperatures and velocities in the two phases. In the VOF model, energy ($E$) and temperature ($T$) are treated as mass-averaged variables:

$$E = \frac{\sum_{q=1}^{n} \alpha_q \rho_q E_q}{\sum_{q=1}^{n} \alpha_q \rho_q}, \tag{7}$$

where $E_q$ is based on the specific heat of the $q^{th}$ phase and the shared temperature.

Evaporation and condensation at the interface are modeled as a source term in the continuity equation for the volume fraction (Eq. 4), i.e.:

$$S_{\alpha_q} = \dot{\mathbf{m}}_i \cdot \mathbf{A}_i \,, \tag{8}$$

where $\mathbf{A}_i$ is an interfacial area density vector, and $\dot{\mathbf{m}}_i$ is a mass flux vector, which for near equilibrium conditions can be determined based on the Schrage[7] equation:

$$|\dot{\mathbf{m}}| = \left(\frac{2\sigma}{2-\sigma}\right)\left(\frac{M}{2\pi R}\right)^{1/2}\left(\frac{P_i}{T_i^{1/2}} - \frac{P_v}{T_v^{1/2}}\right). \tag{9}$$

Here $\sigma$ is the accommodation coefficient (AC); $M$ is the molar mass of the fluid; $R$ is the universal gas constant; $P_i$ and $P_v$ are, respectively, the interfacial and vapor pressures (it was assumed that $P_i \cong P_{sat}$); $T_i$ and $T_v$ are, respectively, the interfacial and vapor temperatures (it was assumed that $T_i = T_v \cong T_{sat}$ at the interface). Finally, $\mathbf{A_i}$ is defined as:

$$\mathbf{A}_i = |\nabla \alpha|, \tag{10}$$

where $\alpha$ is the volume fraction of the primary phase.

In the present implementation, the surface tension forces at the interface are modeled via the Continuum Surface Force (CSF) model of Brackbill et al.[8]. In this model, the surface tension forces at the interface are transformed into a volume force ($\mathbf{F}_{vol}$), which is added as a source to the momentum equation:

$$\mathbf{F}_{vol} = \sum_{pairs\ ij, i<j} \sigma_{ij} \frac{\alpha_i \rho_i r_i \nabla \alpha_j + \alpha_j \rho_j r_j \nabla \alpha_i}{\frac{1}{2}(\rho_i + \rho_j)}\,, \tag{11}$$

where $r_i$ is the surface curvature calculated from the local gradients in the surface normal at the interface:

$$r_i = \nabla \cdot \hat{\mathbf{n}}. \tag{12}$$

### C. Sharp Interface Model

In the SI-CFD model, the governing equations are solved separately for the liquid and vapor domains. The two phases are coupled at the interface through the continuity of velocities and shear stresses, as well as an energy balance performed at the interface boundary:

$$\left|\dot{\mathbf{m}}\right| L = \mathbf{q}_{il} - \mathbf{q}_{iv}\,. \tag{13}$$

Here $\left|\dot{\mathbf{m}}\right|$ is an interfacial mass transfer rate determined from the previously defined Schrage equation (Eq. 9); $\mathbf{q}_{il}$ and $\mathbf{q}_{iv}$ are conductive heat fluxes on the liquid and vapor sides of the interface:

$$\mathbf{q}_{il} = -k_{l\_eff} \nabla T\,|_l \tag{14}$$

$$\mathbf{q}_{iv} = -k_{v\_eff} \nabla T\,|_v \tag{15}$$

In this approach, the interfacial temperature is determined from (13) and essentially approaches saturation temperature only when mass transfer is small, i.e. at near equilibrium conditions.

In order to ensure velocity continuity at the interface, the tangential velocity component on the vapor side of the interface is set equal to the one from the liquid side:

$$v_{tang\_v} = v_{tang\_l}, \tag{16}$$

and the tangential component of the interfacial shear stress from the vapor side is applied to the liquid side of the interface:

$$\tau_{tang\_l} = \tau_{tang\_v} \tag{17}$$

### D. Turbulence modeling

In this study, the tank turbulence was modeled by utilizing the Shear Stress Transport $k$-$\omega$ model of Menter[9] (kw-SST). This model is similar to the standard $k$-$\omega$ model of Wilcox[10] but has the ability to account for the transport of the principal shear stress in adverse pressure gradient boundary layers. These features make the kw-SST model more accurate and reliable for a wider class of flows than the standard $k$-$\omega$ model.

In the VOF model, continuity of the turbulent quantities is inherently assumed since one set of equations for the turbulent kinetic energy and dissipation rate is solved for both phases throughout the domain, with properties varying according to the local volume fraction value.

## IV. Numerical Implementation

In this study a 1.7 m diameter, 2.35 m tall tank known as the Engineering Development Unit (EDU) was considered. The tank has a cylindrical central section and dome shaped top and bottom sections. Axisymmetric 2D tank geometry, which consists of fluid inside the tank, the tank wall and top diffuser used in CFD calculations is shown in Figure 2.

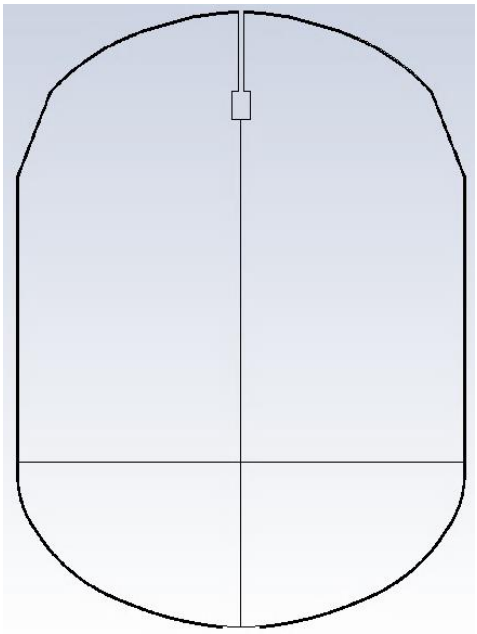

**Figure 2: EDU tank geometry used for calculations**

### E. Autogenous pressurization

In the autogenous pressurization cases initial tank pressure is set to the measured value of 101,270.0 Pa. Measured fluid temperatures before the beginning of the pressurization test are used as the initial temperature conditions for CFD runs, as shown in Fig. 3-a. In CFD liquid temperatures are set to the saturation value (77.35 K) at the initial tank pressure and the temperature profile in the vapor is set to match the measured values. An initial fill level of 26% is used in this study. In the cases where turbulence models are used, initial values for turbulence kinetic energy and specific dissipation rate are set, respectively, to 1e-06, $m^2/s^2$ and 100, 1/s. The tank wall is included in the calculations. The outside surface of the tank wall is modeled as an adiabatic boundary. A small amount of heat coming through the MLI is ignored since a separate simulation showed that applying the heat flux estimated in the experiment didn't have

a significant effect on the tank pressure and temperatures. The contact angle between the liquid and tank wall is assumed to be 0 degrees. No slip boundary conditions are applied on the inside of the tank wall in contact with the fluid. Gaseous nitrogen is injected at the vertical portion of the top injector. Measured time dependent values of the mass flow rate and temperature are applied uniformly at the inlet surface, which is modeled as a mass flow inlet.

The phase change fluids in the tank were liquid nitrogen (LN2) and its vapor. Constant material properties at T_initial = 77.35 K and P_initial = 101270 Pa are used for the phase change fluid, except for $C_p$, thermal conductivity $k$ and viscosity $\mu$, which were represented by temperature-dependent piecewise-linear equations. These properties are summarized in Table 1.

**Table 1: N2 properties from NIST at T_initial = 77.35 K and P_initial = 101270 Pa**

| Property | Units | liquid | vapor |
|---|---|---|---|
| Density | kg/m$^3$ | 806.11 | Ideal gas |
| $C_p$ | J/kg-K | func(T) | func(T) |
| Thermal Conductivity | W/m-K | func(T) | func(T) |
| Viscosity | Pa*s | func(T) | func(T) |
| Surface Tension | N/m | 0.008876 | |
| Thermal Expansion coeff. | 1/K | 0.00567 | - |
| Molecular Weight | kg/kmol | 28.013 | |

### F. Draining

In the draining cases the initial tank pressure is set to the measured value of 246,797.8 Pa. Measured fluid temperatures before the beginning of draining, that were used to obtain initial temperature conditions for CFD runs, are shown in Fig. 3-b. In this case the liquid is stratified prior to tank draining and, therefore, both liquid and vapor temperature profiles are set to match the measured values. The initial fill level for this test was 28%. and the diffuser is turned off. In the experiment, LN2 was removed through the LAD screens. Since it is not possible to include 3D LAD geometry into a 2D axisymmetric model used in the current study, a sump geometry (opening diameter = 0.1463 m) is used to represent the tank outlet. Capacitance probe data is used to estimate the mass flow rate during the draining operation. In CFD, a velocity outlet B.C. is used at the outlet with velocities calculated from the mass flow rate curve fit.

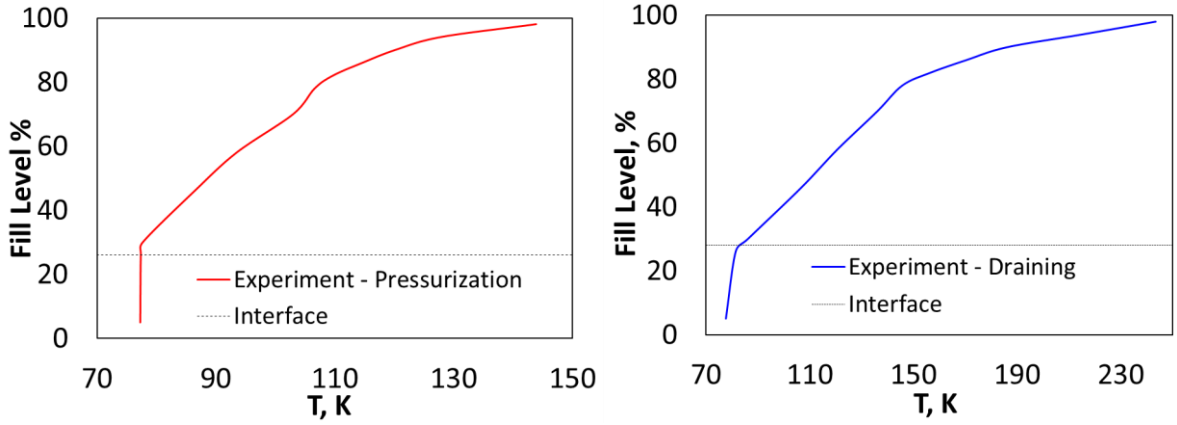


**Figure 3: Measured initial fluid temperatures – a) pressurization; b) draining**

In the draining cases constant material properties at T_initial = 85.79 K and P_initial = 246797.8 Pa are used for the phase change fluid, except for $C_p$, thermal conductivity, and viscosity, which are represented by temperature-dependent piecewise-linear equations. The properties are summarized in Table 2. The tank wall material, Aluminum 2219, is modeled with temperature dependent $C_p$ and thermal conductivity and constant density equal to 2719 kg/m$^3$.

The Second Order Upwind scheme is used to discretize the turbulence, energy, and momentum equations (cell values). The PISO scheme is used for the pressure-velocity coupling (cell values). The Least Squares Cell Based scheme is used for the gradient calculations (face values). The PRESTO! scheme is used for the pressure interpolation (face values). The Point Implicit (Gauss-Seidel) linear equation solver with the Algebraic Multi-Grid (AMG) method

is used to solve the linearized systems of equations. The First Order Implicit temporal discretization and the Geometric Reconstruction scheme for the VOF equation is used with the explicit VOF model. The Second Order Implicit temporal discretization and the Compressive scheme for the VOF equation was used with the implicit VOF model. The convergence criteria are set to $1x10^{-4}$ for all the equations except the energy equation, for which it is set to $1x10^{-6}$. Time step size value of 0.01 seconds is used for both the Sharp Interface and VOF models.

**Table 2: N2 properties from NIST at T_initial = 85.79 K and P_initial = 246797.8 Pa**

| Property | Units | liquid | vapor |
|---|---|---|---|
| Density | $kg/m^3$ | 766.26 | Ideal gas |
| $C_p$ | J/kg-K | func(T) | func(T) |
| Thermal Conductivity | W/m-K | func(T) | func(T) |
| Viscosity | Pa*s | func(T) | func(T) |
| Surface Tension | N/m | 0.00699 | |
| Thermal Expansion coeff. | 1/K | 0.0065311 | - |
| Molecular Weight | kg/kmol | 28.013 | |

## G. Computational mesh

Two different 2D axisymmetric computational grids are used in the current study. Their characteristics are summarized in Table 3. These grids are shown in Fig. 4. The main difference between these grids is that Grid 1 (Fig. 4-a) has highly stretched cells along the liquid-vapor interface unlike Grid 2 (Fig. 4-b), which has orthogonal cells near the interface. Grid 1 has finer mesh near the tank wall and next to the interface. Comparison between the two meshes in terms of predicted tank pressures is presented in the "Results and Discussion" section of this paper.

**Table 3: Mesh Characteristics**

| **Name** | **Grid 1** | **Grid 2** |
|---|---|---|
| First cell at | 0.05 mm | 0.5 mm |
| Number of cells | 34,500 | 27,000 |

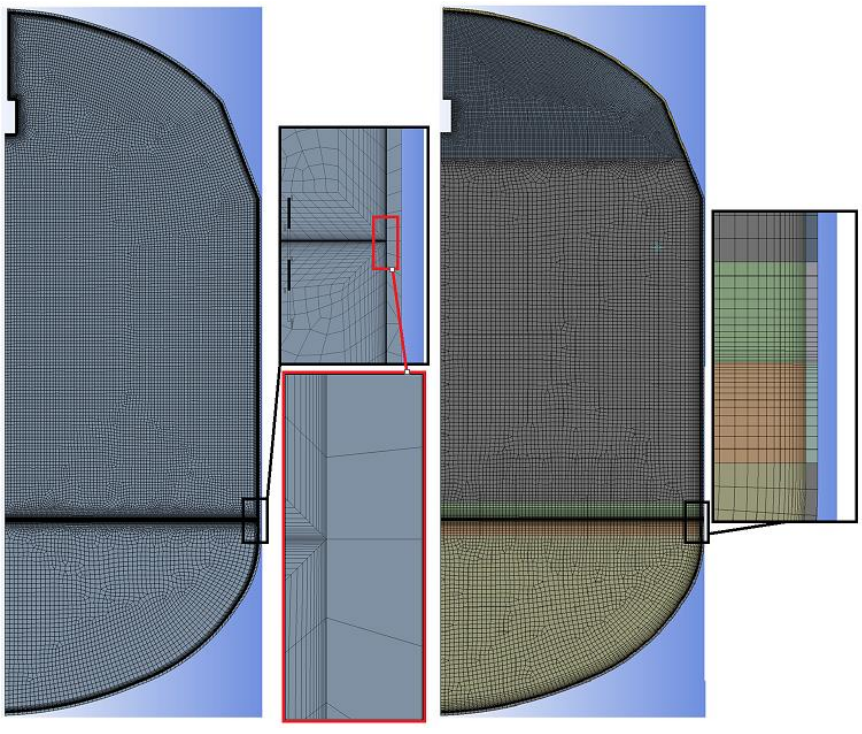

**a)** **b)**

**Figure 4: Computational grids – a) Grid 1; b) Grid 2**

## V.Results and Discussion

In this section, results of CFD simulations are presented and compared with the experiemntal data obtained in the EDU experiment. The autogenous pressurization results are discussed first, followed by a discussion of the draining simulations results.

### H. Autogenous pressurization

Tank pressures predicted using two different computational grids, shown in Fig. 4, are compared with the experimental data in Fig. 5. The resulting pressures are essentially the same for both grids, which indicates that additional grid refinement below 0.5 mm at the interface is not necessary in this case. Therefore, Grid 2 was used in all of the following simulations.

A study of the effect of the Accommodation Coefficient (AC) with the SI-CFD model was conducted next. Predicted tank pressures are compared with the experimental data in Fig. 6. The values of AC studied are: 1, 1e-2, 1e-4, 1e-8 and 0. Models with the values of AC = 1, 1e-2 and 1e-4 predict similar tank pressures and condensation phase change rates (not shown in this paper). Models with AC = 1e-8 and 0 predict no condensation and the tank pressures for these two cases match.

The effects of turbulence - and interfacial phase change were studied. Tank pressures predicted by the turbulent and laminar Sharp Interface models with phase change and the laminar model without phase change are compared with the experimental data in Fig. 7. Both the turbulent and laminar SI-CFD models predict very similar tank pressures which match the experimental data well. The model without phase change (No-MT) predicts higher tank pressures compared to the models with phase change and experimental data. This was expected since condensation phase chage reduces tank pressure. Phase change rates predicted by the laminar and turbulent SI-CFD models are compared in Fig. 8. Both models predict condensation which rate is increasing during the test. The values of the phase change rate predicted by the two models are very similar.

Fluid temperatures predicted by the laminar SI-VOF are compared with the experimental data in Fig. 9Figure . As shown in the figure, liquid and vapor temperatures up to 58 percent fill level location match experimental data well.Temperatures at the top of the vapor region at and above the 70% fill level location are under-predicted in CFD compared to the experimental values. Fluid temperatures predicted by the turbulent (k-omega SST) SI-CFD model are compared with the experimental data in Fig. 10. In this case, just like in the case with the Laminar model, liquid and vapor temperatures up to 58 percent fill level location match experimental data well. Temperatures at the top of the vapor region at and above 70% fill level location are under-predicted in CFD compared to experimental values. The turbulent model predicts less fluctuations in fluid temperatures compared to the Laminar model.

Temperature contours and streamlines in the vapor and liquid regions are compared between the laminar and turbulent Sharp Interface model results in Fig. 11 at 1600 seconds after the beginning of simulation. Temperature contours predicted by the two models are very similar, except at the top of the tank, where the laminar model predicts higher vapor temperatures, compared to the results of the turbulent model. The turbulent model predicts a recirculation zone at the top of the tank – at and above the diffuser level. On the other hand, the laminar model predicts several large vortices in the vapor region. In the liquid region both models predict two large recirculation zones – one near the interface, mixing the top layer of liquid; and one near the bottom of the tank.

Tank pressures predicted by the SI-CFD and VOF-CFD multiphase models during pressurization are compared with the experimental data in Fig. 12-a. Both models predict very similar tank pressure increases during pressurization that are in an exlllent agreement with the experiemntal data. Both are within 2.5% of the experimental value, as shown in Fig. 12-b. This is in contrast to the results of the models presented by Ciccotosto and Hauser[4], who showed that the VOF model significantly underpredicted tank pressure during pressurization (up to 24% of the experimental value). Their laminar Sharp Interface model predicted tank pressures that are in a good agreement with the experiemntal data (within 1.4% of the experimental data).

Fluid temperatures predicted by the VOF-CFD model are compared with the experimental data in Fig. 13. Monitor points locations are shown in Fig. 13 for reference. These results, that are very similar to the SI-CFD model results (presented in Fig. 9), show that liquid and vapor temperatures up to the 70% fill level location match experimental data well. Temperatures at the top of the vapor region at and above 78% fill level location are under predicted by this model. The lack of good temperature agreement in the upper tank region is attributed to the fact that heat transfer from the diffuser (heated by the hot gas) to the vapor region was not included in the present model. Furthermore, due to the 2D axisymmetric assumption and other simplifications applied to the diffuser, important details of the injector geometry were omitted in CFD models.

Temperatures and streamlines in the tank at 1600 seconds after the beginning of pressurization are compared between the VOF-CFD and SI-CFD models in Fig. 14. Both models indicate that hot diffuser flow is mixing the top

of the vapor region, while the rest of the vapor region is stratified, and the liquid region is cold. Streamlines show mixing in the ullage which helps to slowly bring warmer temperatures from the top of the tank near the diffuser towards the interface. The SI-CFD model predicts two separate recirculation zones in the liquid – one near the interface and another at the bottom of the tank. In the VOF model these recirculation zones are less distinct.

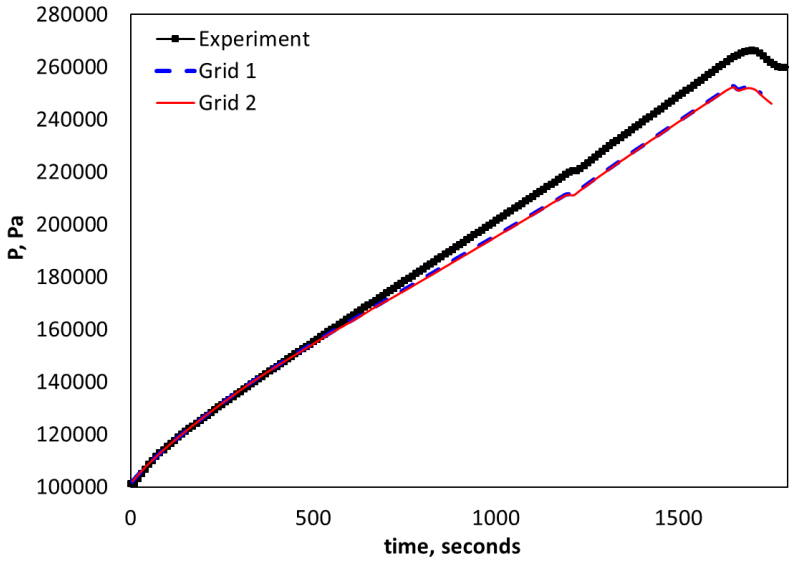


**Figure 5: Grid comparison**

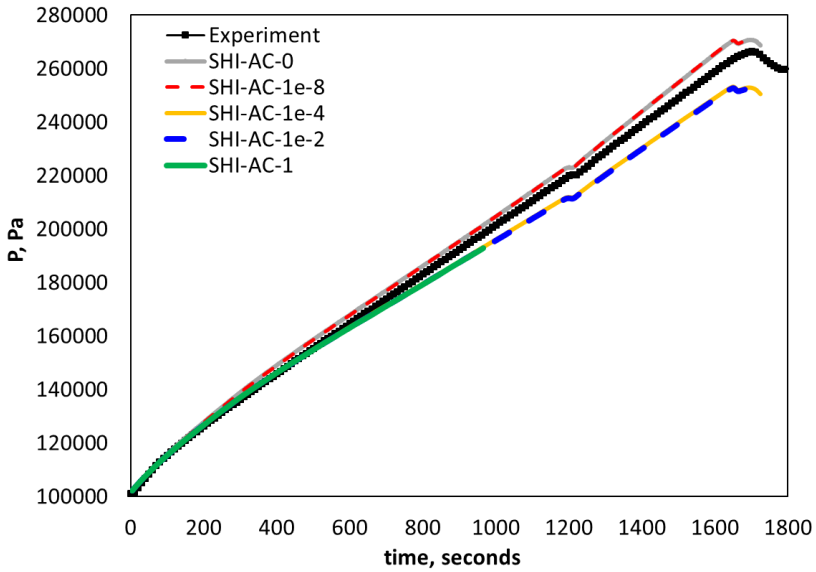


**Figure 6: Autogenous Pressurization - Effect of Accommodation Coefficient (AC) with the SI-CFD model – Tank Pressure**

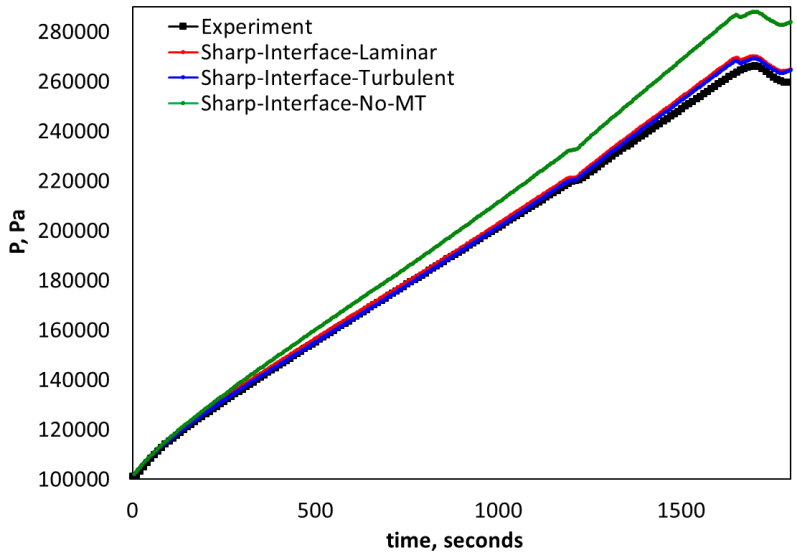


**Figure 7: Autogenous Pressurization - SI-CFD model – effect of turbulence modeling and phase change - tank pressure**

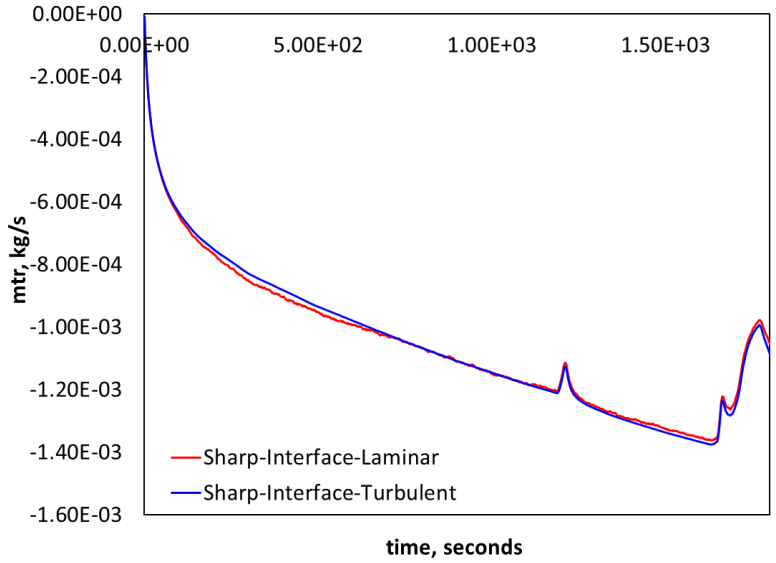


**Figure 8: Autogenous Pressurization SI-CFD model - effect of turbulence modeling - phase change rate**

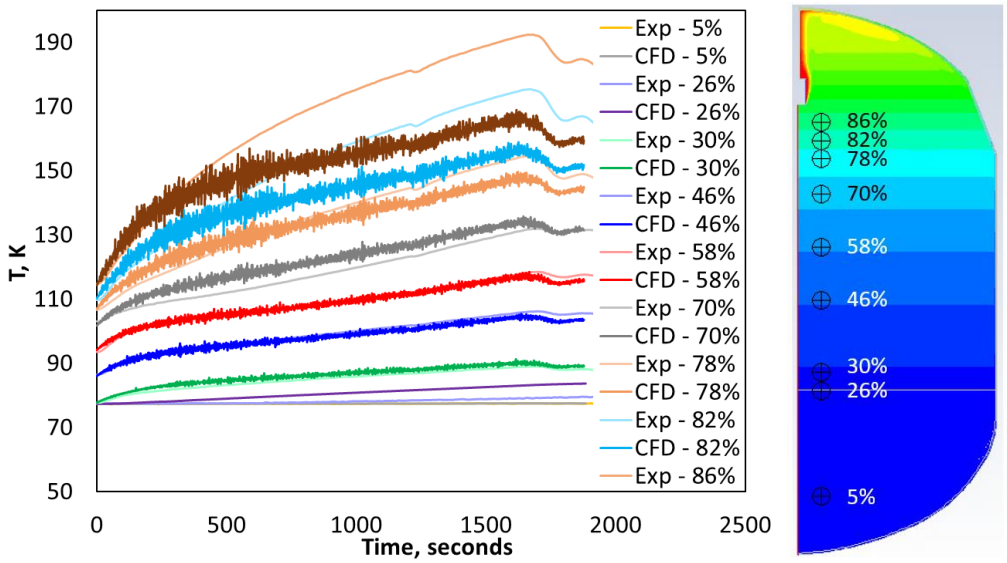


**Figure 9: Autogenous Pressurization - Fluid temperatures predicted by the laminar SI-CFD model at different tank heights compared with the experimental data**

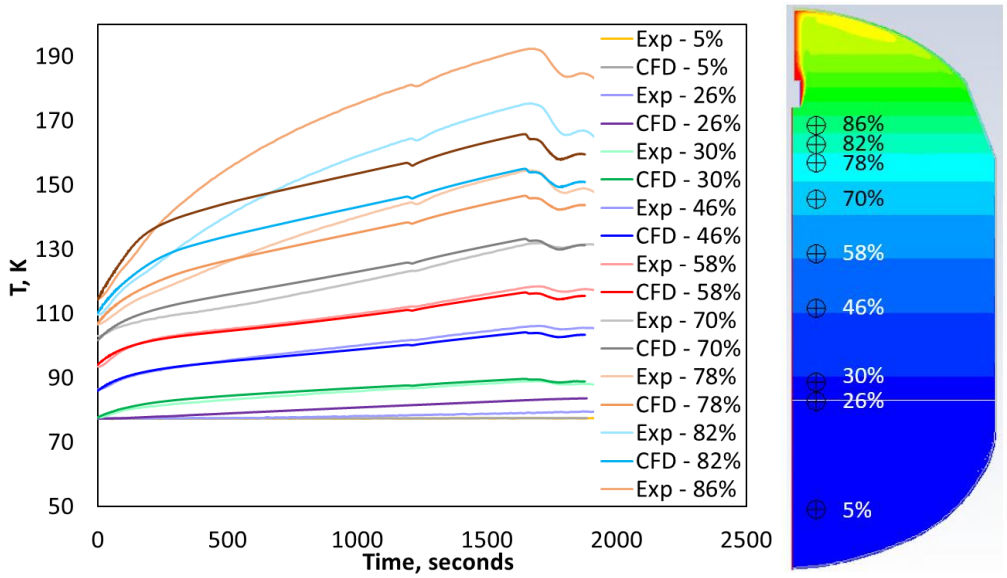


**Figure 10: Autogenous Pressurization - Fluid temperatures predicted by the turbulent SI-CFD model at different tank heights compared with the experimental data**

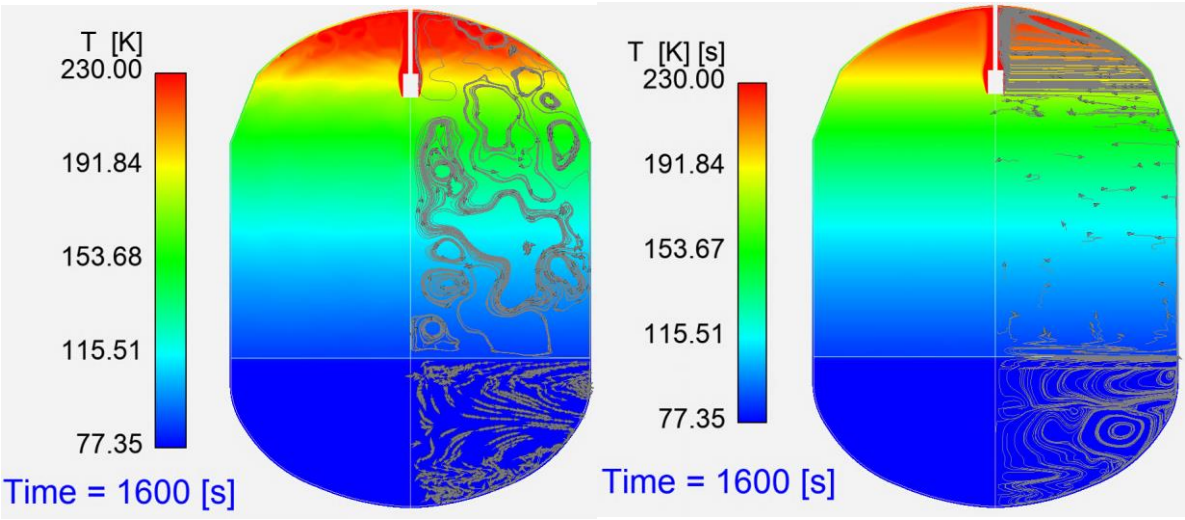


**Laminar** **Turbulent**

**Figure 11: Autogenous Pressurization - Laminar vs. Turbulent SI-CFD model results – temperature contours and streamlines at 1600 s**

**I. Draining**

The initial and final phase distributions in the tank, predicted by the VOF-CFD and SI-CFD models are shown in Figs. 15-a and 15-b respectively. As can be seen in the figure, the predicted liquid volume (blue region) decrease in the tank during the 350 seconds of draining is similar between the two models. Figure 15-c shows the mesh and position of the liquid-vapor interface in the beginning and at the end of the simulation [the line between the blue (liquid) and red (vapor) regions] as predicted by the SI-CFD model with an enhanced capability of moving the mesh with the movement of the interface.

The predicted tank pressure responses during draining are compared between the SI-CFD and VOF-CFD models and with the experimental data in Fig. 16-a. Figure 16-b shows the percent difference between the predicted and measured tank pressures and Fig. 16-c presents predicted vs. experimental pressure rise rates. The SI-CFD model with moving interface predicts tank pressures that match the VOF model results. Both models predict the slope of the tank pressure decrease that matches the experimental data for most of the run, except in the first 100 seconds of draining, where CFD models are predicting a slower rate compared to the experimental pressure decrease. This could be because in the experiment the tank was pressurized, and the valve was closed right before the draining portion started, in the CFD case, this portion of the test was not modeled. The effect of pressurization prior to draining might have influenced the condensation phase change rate and, therefore, tank pressure. Both models, as shown in Fig. 16-b, predict tank pressures during draining that are within 3.5% of the values measured in the experiment.

Liquid and vapor temperatures predicted by the Sharp Interface model are compared with the experimental data in Fig. 17 for temperature probes located between 5% and 58% fill levels. Predicted liquid temperatures (up to 22% fill level) are in a very good agreement with the experimental data. During draining the 30% fill level location is originally right above the liquid-vapor interface (28%). Temperatures at 30% fill level location are under-predicted by the SI-CFD model. This could be due to the fact that the moving interface produces some interface deformation and, in turn, increased mixing right above the interface that could result in higher temperatures. In the SI-CFD model with moving interface, the interface - remains rigid and undeformed while moving. CFD results are in a good agreement with measured vales at higher 46% and 58% fill level locations.

A comparison between the phase change rates predicted by the SI-CFD and VOF-CFD models is presented in Fig. 18. Both models predict initial condensation for the first 160 seconds of draining followed by evaporation at the interface. The VOF-CFD model predicts more condensation and larger oscillations in the phase change rate compared to the results of the SI-CFD model.

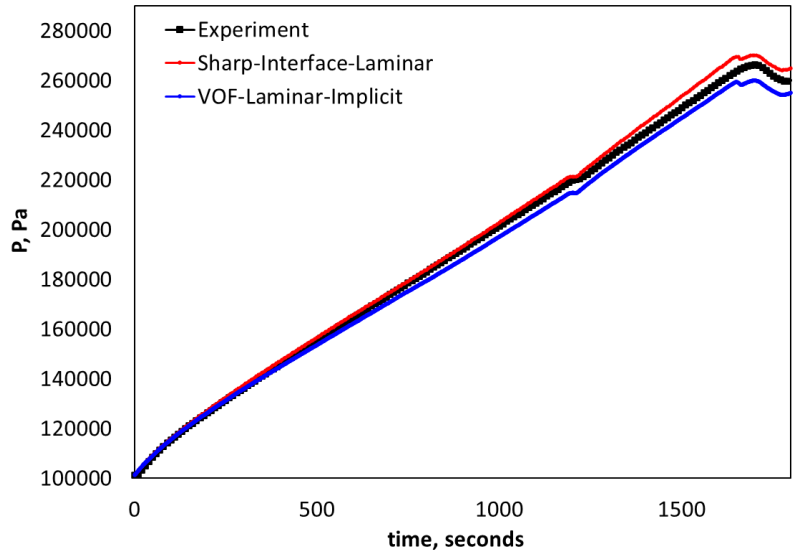


**a) tank pressure**

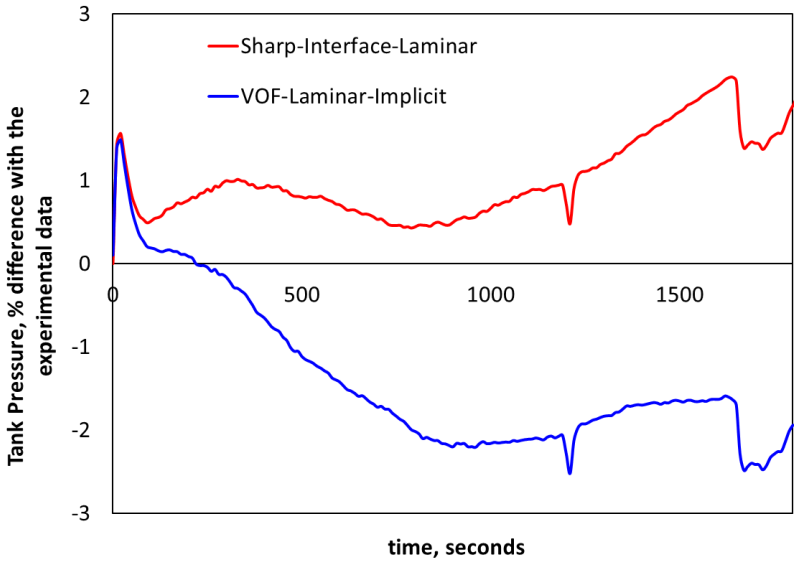


**b) % difference between predicted and measured tank pressure**

**Figure 12: Autogenous Pressurization – a) tank pressure; b) % difference between predicted and measured tank pressure**

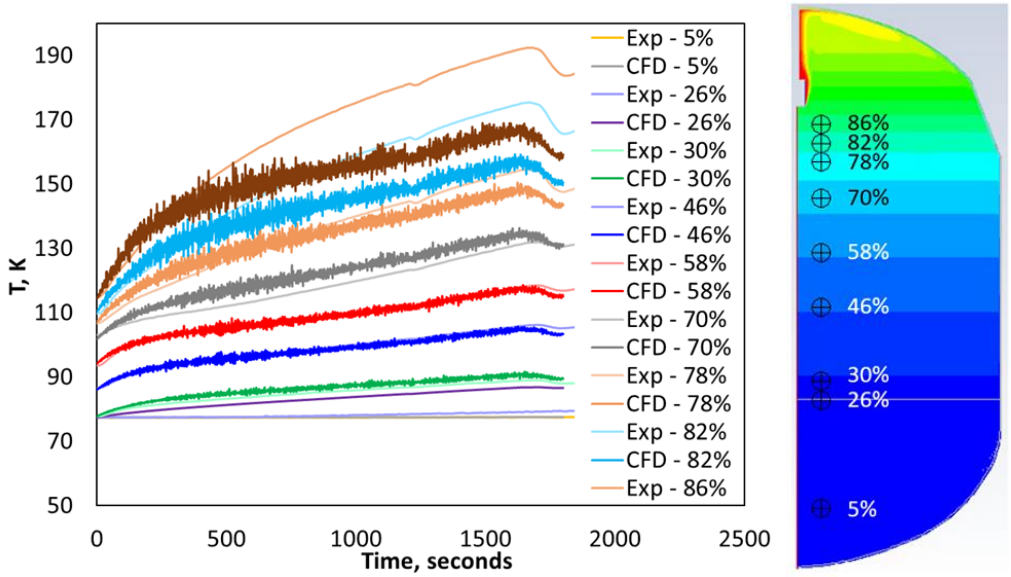


**Figure 13: Autogenous Pressurization - Laminar Implicit VOF-CFD model - fluid temperatures**

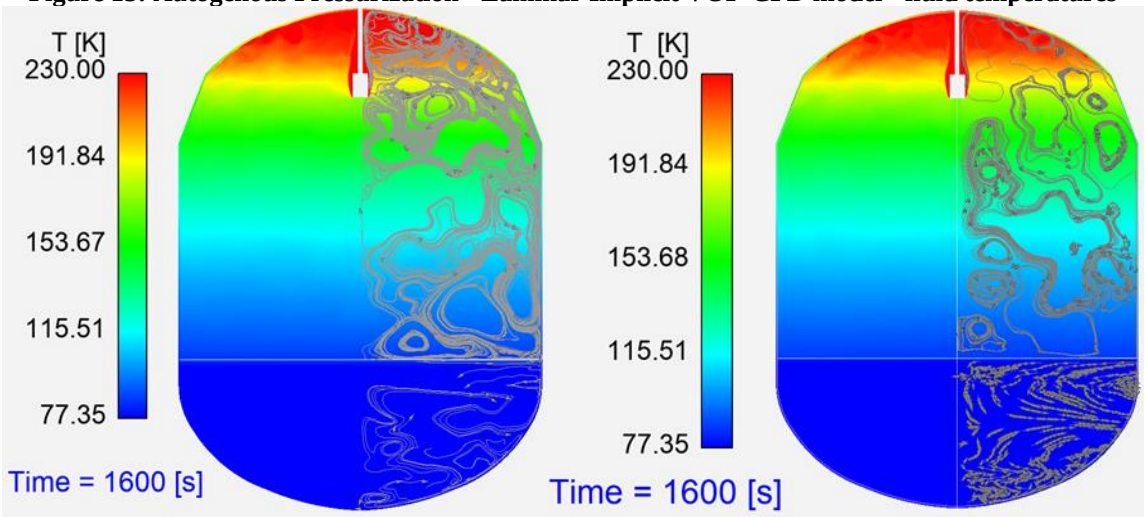


**VOF** **Sharp Interface**

**Figure 14: Autogenous Pressurization - Temperatures and streamlines in the tank at 1600 seconds of simulation time: Comparison between the laminar VOF_CFD and SI-CFD models**

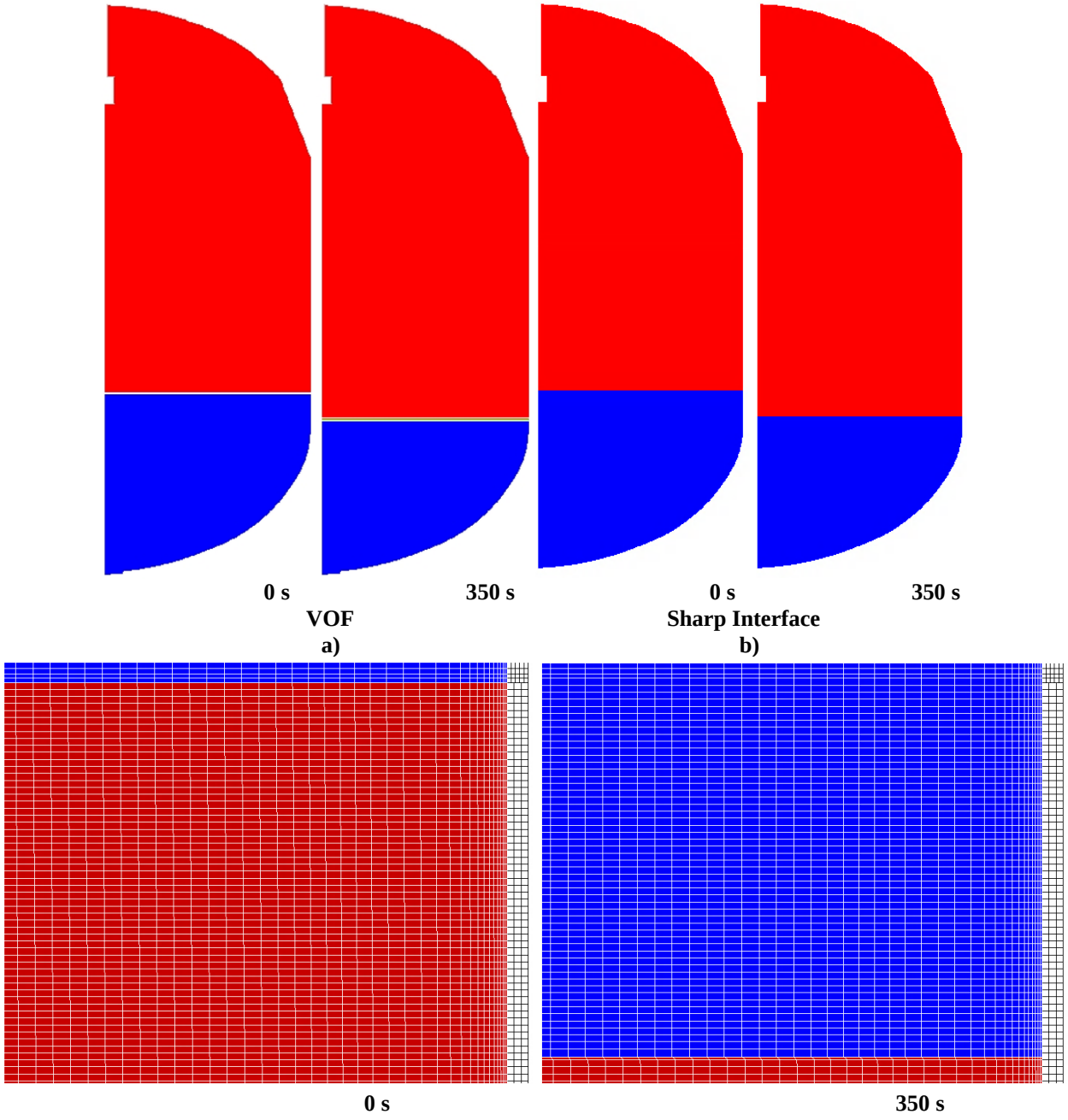


**Figure 15: EDU tank draining – VOF-CFD and SI-CFD model predictions – phase distribution**

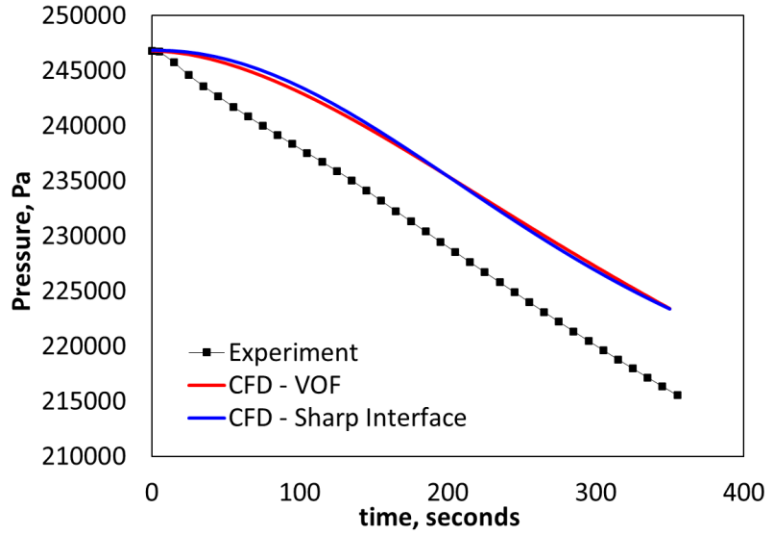


**a) tank pressure**

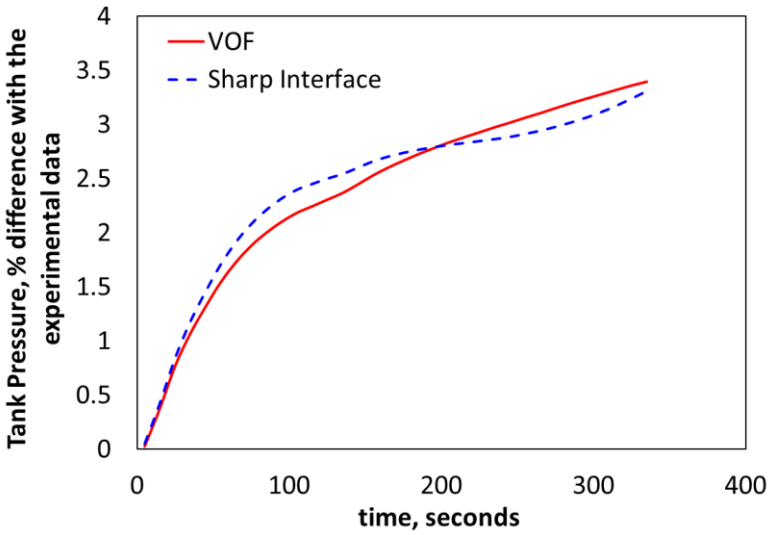


**b) % difference between predicted and measured tank pressure**

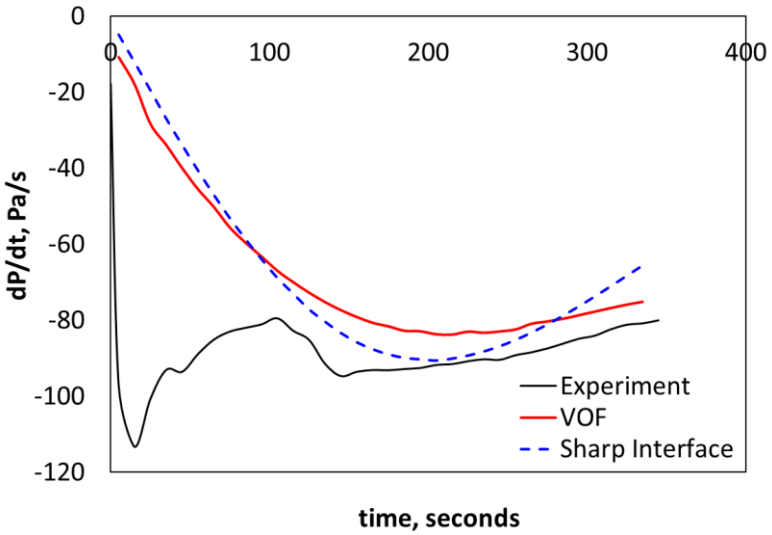


**c) predicted and experimental pressure rise rates**

**Figure 16: Draining – a) tank pressure; b) % difference between predicted and measured tank pressure; c) predicted vs. experimental pressure rise rates**

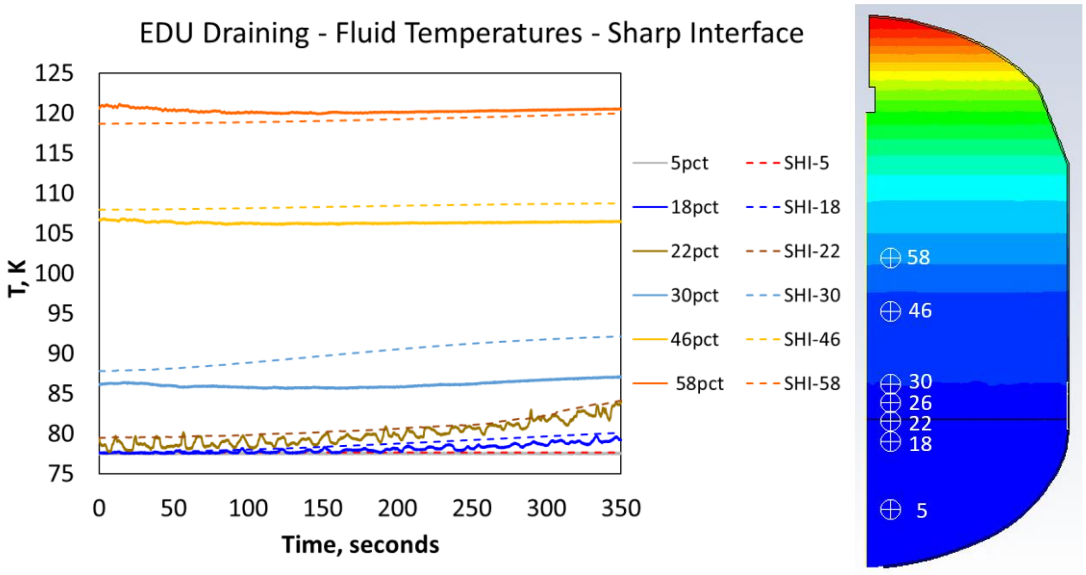


**Figure 17: EDU tank draining – SI-CFD model - fluid temperatures**

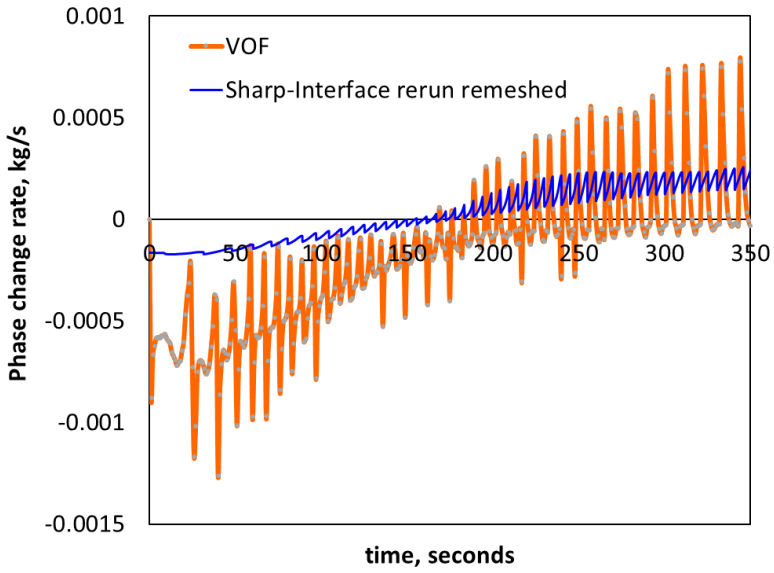


**Figure 18: EDU tank draining - Comparison between the phase change rates predicted by the SI-CFD- and VOF-CFD models**

## VI. Conclusion

CFD results for autogenous pressurization and draining of a cryogenic storage tank in normal gravity are presented in this paper. To assess the fidelity of the CFD models, predicted tank pressure and fluid temperatures are compared with data provided by the Engineering Development Unit (EDU) experiments. Two different methods of modeling the phase front and the associated interfacial heat, mass and momentum transfer between the liquid and vapor regions are used in this study. These are the Sharp Interface and VOF methods.

In the autogenous pressurization study the results of the laminar Sharp Interface model are compared with the results of the laminar VOF model and experimental data. Tank pressures predicted by both multiphase models are within 3% of the experimental data. Similarly, to the results of the Sharp Interface model, the VOF model predicts fluid temperatures in the liquid region and in the lower to middle vapor regions well. Both multiphase models under-predict temperatures in the upper region of the vapor in the tank, close to the diffuser. The effects of computational

mesh and accommodation coefficient (AC), used for predicting phase change with the SI-CFD are assessed. The results of this assessment show that predicted tank pressure during pressurization is independent of the value of AC used, unless a very low value (1e-8 or 0) is used. The assessment of the computational grid effect showed that additional grid refinement below 0.5 mm at the interface is not necessary in this case.

A Sharp Interface model with moving liquid-vapor interface boundary was developed and validated against the draining portion of the EDU experiment. The VOF model was also used to simulate tank draining and its results were compared with the results of the Sharp Interface model with moving interface. Both models predict the slope of the tank pressure decrease well, matching the experimental data after 100 seconds after the beginning of the draining period. However, both models, predict slower pressure decrease in the beginning of draining compared to the experimental data. This may be due to the fact that the gaseous pressurization was stopped right before the draining in the experiment, but this was not reflected in CFD simulations. Tank pressure values predicted by both models are within 3.5% of the experimental data. Fluid temperatures predicted by the Sharp Interface model with moving interface boundary are in a good agreement with the experimental data. Both, the Sharp Interface and VOF models predict initially net condensation that changes to evaporation after 150-200 seconds of draining.

The Sharp Interface and VOF models with phase change implemented in ANSYS Fluent CFD code were successfully verified and validated in this study against EDU GN2 autogenous pressurization and tank draining experiments in normal gravity. The Sharp Interface model with moving liquid-vapor interface boundary, developed for tank draining, was also successfully applied and validated.

## Acknowledgments

Authors would like to thank the Modeling Portfolio Project within the STMD CFM Project Office for providing funding for this work and Dan White who provided tank geometry, initial and boundary conditions and initial CFD case setup.

## References

[1] T. Page “Thermal Test Report and Thermal Math Model Test Correlation Report for the Cryogenic Propellant Storage and Transfer (CPST) Engineering Development Unit (EDU)” NASA report EV34-19-002, NASA Marshall Space Flight Center, August 2019

[2] Salzman, J., “Fluid management in space-based systems,” *Proceedings of the Engineering, Construction, and Operations in Space, 5th international conference on space*, Vol. 1, 1996, p. 521–6.

[3] von Rüden, David. (2021). Pressurization Behavior of a Cryogenic Propellant Tank in Microgravity.

[4] B.E., Ciccotosto, D.M., Hauser, “Autogenous Pressurization of a Cryogenic Tank using Computational Fluid Dynamics”, Proceedings of the AIAA Propulsion and Energy Forum, August 2021, Virtual, AIAA2021-3558

[5] P., Adnani, R., Jennings, “Pressurization analysis of cryogenic propulsion systems”, Proceedings of the 36th AIAA/ASME/SAE/ASEE Joint Propulsion Conference and Exhibit, July 2000, Las Vegas, NV, AIAA2000-3788

[6] C.W. Hirt and B.D. Nichols, “*Volume of fluid (VOF) method for the dynamics of free boundaries*”, *Journal of Computational Physics* **39** (1): 201-225. 1981.

[7] R.W. Schrage, A theoretical study of interphase mass transfer, Columbia University Press, New York, 1953.

[8] Brackbill J.U., Kothe, D.B., Zemach, C., “A continuum method for modeling surface tension,” J. Comp. Phys. Vol. 100, 1992, pp. 335–354.

[9] Menter, F. R., “Two-Equation Eddy-Viscosity Turbulence Models for Engineering Applications,” AIAA Journal, 32(8), 1994, pp. 1598-1605.

[10] Wilcox, D.C., *Turbulent Modeling for CFD*, DCW Industries, Inc., La Canada, California, 1998.